Channel Modeling and Interference Analysis in IEEE 802.11a Wireless Communication Systems

Yu Zhang[1], Xinzhe Pi[2], and Meiyun Xie[2]
[1]School of Computer Science and Technology, Xidian University, Xi'an, Shaanxi, 710071, China
[2]School of Systems Information Science, Future University Hakodate, 116-2
Kamedanakano-cho, Hakodate, Hokkaido, 041-8655, Japan

IEEE 802.11a remains a key component for localized connectivity in fifth-generation (5G) networks and is widely used in smart homes, industrial IoT, and public WiFi hotspots. Due to the randomness and dynamic nature of wireless propagation channels, IEEE 802.11a systems are subject to unavoidable interference, including path loss, multipath propagation, shadowing, and Doppler effects. Although numerous studies have addressed signal interference in IEEE 802.11a systems, there is a notable lack of comprehensive overviews on state-of-the-art channel modeling and interference analysis in the existing literature. Specifically, critical challenges such as accurately modeling dynamic channel behaviors and analyzing the impact of the objective interference in wireless channels require further exploration. This paper provides a comprehensive review of channel modeling and interference mechanisms for IEEE 802.11a wireless communication systems. Based on the different sources, we first categorize existing interference into two types: multiplicative interference and additive interference. The former includes large-scale fading caused by path loss and shadowing effects, as well as small-scale fading resulting from multipath propagation and Doppler effects. The latter is further classified into thermal noise, adjacent channel interference, co-channel interference, and electromagnetic interference. Furthermore, we analyze the impact of these interference types on signal characteristics, including amplitude, phase, frequency, and time delay, and identify key gaps in current modeling approaches. Finally, we highlight future research directions, focusing on improving channel modeling techniques, developing interference-aware protocols, and developing cross-layer optimization frameworks for secure and efficient transmission in dynamic network environments.

Index Terms—**Wireless communication system, IEEE 802.11a, channel modeling, interference analysis, physical layer transmission.**

I. Introduction

WIRELESS communication systems have undergone rapid advancements to meet the increasing demand for higher data rates, low latency and seamless connectivity [1]. Driven by the evolution of fifth-generation (5G) and sixth-generation (6G) wireless systems, there has been a significant shift toward integrating diverse wireless standards, including legacy systems such as IEEE 802.11a, to ensure backward compatibility while leveraging existing technologies for specific applications [2]. Utilizing the Orthogonal Frequency Division Multiplexing (OFDM) technique, the IEEE 802.11a system operates in the 5 GHz band to deliver high spectral efficiency and reduce interference relative to the 2.4 GHz band [3]. These features make the IEEE 802.11a system particularly effective in local area networks (LANs) and for offloading traffic from cellular networks in high-density environments. Even as 5G and 6G networks adopt advanced wireless techniques, the IEEE 802.11a system continues to serve as a foundation for wireless LAN (WLAN) connectivity in scenarios requiring localized high-throughput links, such as smart homes, industrial IoT and public WiFi hotspots [4].

Communication channels of IEEE 802.11a systems are inherently subject to unavoidable interference due to the random and dynamic nature of the wireless propagation environment. The interference stem from multiple sources, including multipath propagation, shadowing, Doppler effects, and external interference, resulting in signal degradation and performance fluctuations. Moreover, the higher frequencies utilized in IEEE 802.11a systems pose inherent challenges, including greater attenuation, limited range, and heightened sensitivity to multipath propagation, which collectively degrade signal power, coverage, and reliability, particularly in environments with complex propagation conditions. Therefore, modeling and analysis wireless propagation channels are foundational to improving the performance of IEEE 802.11a systems.

Existing studies have provided significant insights into key channel interference in IEEE 802.11a wireless communication systems, such as channel modeling and fading [5]–[7], adjacent channel interference (ACI) [8], [9], coexistence interference [10]–[12], and OFDM system performance [13], [14]. However, these studies predominantly focus on the impact of individual interference types on system performance, while lacking a systematic and comprehensive framework that examines all interference types and their effects on propagation signals in IEEE 802.11a systems. This limitation hinders a comprehensive understanding of interference mechanisms and restricts the optimization and application of IEEE 802.11a systems in future complex interference environments.

Motivated by these gaps, this paper provides a comprehensive review of the inevitable interference in IEEE 802.11a wireless communication systems and presents the first in-depth analysis of their impact on signal characteristics. In particular, we categorize the interference sources into two primary types: additive interference and multiplicative interference, thereby establishing a unified classification framework. For each type, we analyze its impact on essential signal characteristics, such

Manuscript received December 17, 2024; revised January 24, 2025. Corresponding author: Yu Zhang (email: yuzhang_@stu.xidian.edu.cn), Xinzhe Pi (email: pxinzhe@163.com).

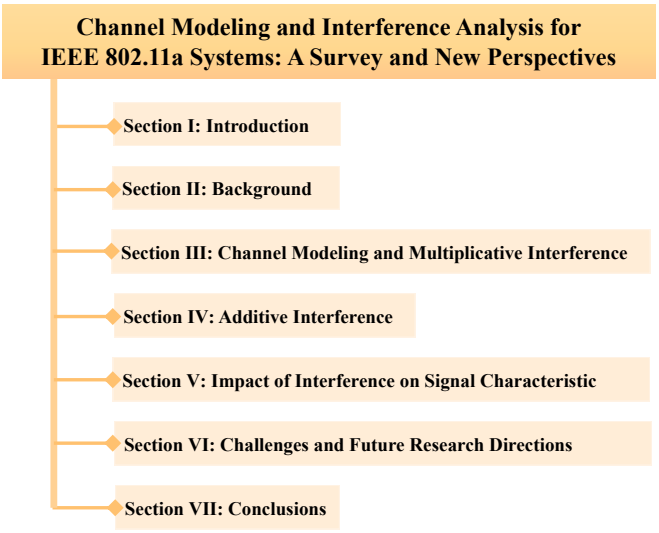

Fig. 1. Organization of this paper.

as amplitude, phase, frequency, and time delay. Finally, we identify key challenges associated with interference analysis in 802.11a systems, including multi-source interference coexistence and dynamic interference prediction, and highlight promising future research directions.

The rest of this paper is organized as follows. Section II introduces the background of channel propagation characteristics and IEEE 802.11a transmission process. Section III presents the channel modeling and multiplicative interference analysis. The additive interference is provided in Section IV. Section V analyzes the impact of interference on signal characteristics. Section VI highlights open problems and future research directions, while Section VII concludes the paper. The organization of this paper is illustrated in Fig. 1.

II. Background

A. Wireless Signal Propagation

Wireless signal propagation is determined by the physical behavior of electromagnetic waves, which carry and modulate information through parameters like amplitude, frequency, phase, and time delay [15]. Electromagnetic waves are a type of wave phenomenon formed by the mutual coupling of electric and magnetic fields. Information is loaded onto the carrier frequency of electromagnetic waves using various modulation techniques for signal transmission. Electromagnetic waves can be theoretically modeled using Maxwell's equations, which provide a formal representation of key propagation phenomena in wireless communication channels, including wave superposition effects, wave diffusion effects, and boundary propagation effects. Each of these phenomena is described below [16].

- **Wave Superposition Effect** Interference is a direct consequence of the principle of wave superposition and relies on the phase and amplitude of multiple electromagnetic waves [17]. When the peaks and troughs of two or more signals align, the intensity of the resulting superimposed signal increases, leading to constructive interference. In contrast, when the peak of one signal aligns with the trough of another, the intensity of the superimposed signal decreases or may cancel out entirely, resulting in destructive interference.
- **Wave Diffusion Effect** Wave diffusion describes the dispersive characteristics of wave propagation in the presence of obstacles and heterogeneous media, leading to deviations in signal paths and attenuation of signal strength. When the size of an obstacle or aperture exceeds the wavelength, large-scale diffraction phenomena occur [18]. Conversely, when the dimensions of scatterers are much smaller than the wavelength, small-scale scattering phenomena arise [19]. The change in refractive index causes the wave direction to shift, as described by Snell's law. This shift in direction is significant in atmospheric propagation, where layered gradients alter signal paths [20].
- **Boundary Propagation Effects** Boundary propagation effects encompass reflection and refraction phenomena, which describe the propagation characteristics of waves in different media. Reflection refers to the phenomenon where part or all of the electromagnetic wave energy is returned to the original medium when the wave encounters the boundary of a medium [21]. Refraction refers to the bending of the wave's propagation direction due to a change in wave speed as the electromagnetic wave passes through the boundary into a new medium [22].

These phenomena impact the instantaneous received signal differently. When a clear Line-of-Sight (LOS) path exists between the mobile device and the base station, diffraction and scattering have minimal effects, and reflection does not dominate signal propagation. In dense urban environments or large metropolitan areas dominated by Non-LoS (NLOS) conditions, diffraction and scattering become the primary mechanisms affecting the signal propagation path [15].

B. IEEE 802.11a Physical Layer Transmission Process

The IEEE 802.11a standard undergoes a comprehensive Physical Layer transmission process to facilitate efficient wireless communication. This process can be broadly categorized into the following stages:

- **Channel Encoding** By adding redundancy for error detection and correction, channel encoding converts data bits into encoded bits.
- **Signal Modulation** Signal modulation converts bit data into symbols using the quadrature phase shift keying (QPSK) or the quadrature amplitude modulation (QAM).
- **Wireless Channel Physical Layer Transmission** At the transmitter, processed data is mapped to OFDM symbols and converted into time-domain signals via the inverse fast Fourier transform (IFFT). The time-domain signals propagate through the wireless channel with various interferences, causing random changes in amplitude, phase, frequency and delay.

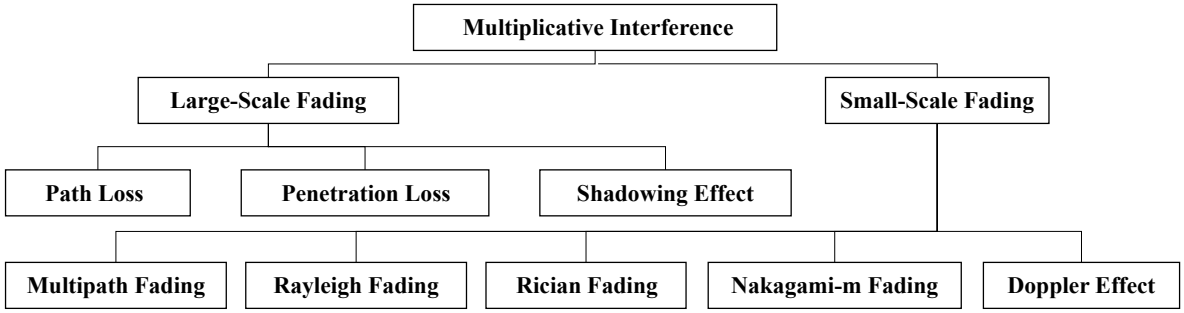

Fig. 2. Different types of multiplicative interference.

- **Signal Demodulation** After channel decoding, OFDM symbols are converted to the frequency domain using FFT.
- **Channel Decoding** The received signals are synchronized and decoded to correct errors from interference and noise during transmission.

In wireless channel propagation, signal impairments can be categorized into two primary types: multiplicative interference and additive interference. Additive interference is regarded as background noise inherent to the propagation environment and persist regardless of whether a signal is being transmitted. These perturbations contribute to the overall noise floor, affecting the signal-to-noise ratio (SNR) and potentially degrading the quality of the received signal. In contrast, multiplicative interference depends on the signal's propagation behavior. These impairments arise from phenomena such as fading, shadowing, and multipath propagation, where the signal's amplitude and phase are altered due to interactions with the environment. Therefore, the signal transmission process through the wireless channel can be modeled as

$$Y_m = C_m X_m + W_m, \tag{1}$$

where Y_m denotes the received signal at subcarrier m and X_m denotes the transmitted signal. The channel response C_m is determined by the multiplicative interference generated during signal propagation. The term W_m represents the effects of the additive interference, which is typically modeled as additive white Gaussian noise (AWGN).

III. Channel Modeling and Multiplicative Interference

Channel modeling aims to characterize the time-varying and frequency-selective characteristics of signals during propagation. These characteristics constitute the channel state information (CSI), which represents a combination of various multiplicative interferences. Based on the different scopes and variation rates, the multiplicative interferences can be further classified into large-scale fading and small-scale fading, as shown in Fig. 2. Detailed descriptions are provided in the following subsections.

A. Large-Scale Fading

Large-scale fading exhibits a slow-varying nature and results in a reduction in the average signal power over large spatial and temporal scales. In IEEE 802.11a systems operating in the 5 GHz band, large-scale path loss is primarily determined by path loss, penetration loss, and shadowing effects. Since the frequency of 5 GHz is higher than that of 2.4 GHz, the shorter wavelength of 5 GHz signals leads to greater penetration loss when passing through walls and other obstacles, resulting in higher overall path loss.

1) Free-Space Path Loss

The free-space path loss (FSPL) describes the theoretical minimum path loss for the a signal propagating through free space due to the spreading of electromagnetic wavefronts [23]. It assumes ideal LoS conditions without obstacles, reflections, or atmospheric effects. The FSPL in decibels (dB) is mathematically expressed as

$$PL_{fspl}(d, f) = 20\log_{10}(d) + 20\log_{10}(f) + 32.44 - G_t - G_r, \tag{2}$$

d is the distance between the transmitter and receiver, f is the carrier frequency in megahertz (MHz), G_t and G_r represent the transmitter and receiver antenna gains in decibels (dB), respectively, and 32.44 is a constant that accounts for the unit conversion from meters and Hertz to kilometers and megahertz. For higher frequencies, such as the 5 GHz band used in IEEE 802.11a, this model predicts significant attenuation, which is important for network planning in high-frequency systems.

2) General One-Slope Path Loss

The general one-slope (OS) path loss establishes a linear relationship between the path loss and the logarithm of the distance d between the transmitter and receiver [24]. It is typically used as a baseline for estimating path loss in environments with little obstruction. The basic form of the one-slope path loss PL_{os} at a distance d is given by:

$$PL_{os}(d) = l_0 + 10 \cdot \gamma \cdot \log_{10}\left(\frac{d}{d_0}\right), \tag{3}$$

where l_0 is the reference path loss at a reference distance d_0, γ is the path loss exponent, which depends on the environment (typically ranging from 2 in free space to 4 or more in urban environments), and d_0 is the reference distance, often set to 1 meter. This model is straightforward and easy to implement,

but it does not account for the impact of different propagation environments over varying distances.

3) Modified Two-Slope Path Loss

Breakpoints in wireless propagation divide the channel into two regions with distinct propagation characteristics [25]. Before the breakpoint, signal attenuation occurs gradually with increasing distance. However, beyond the breakpoint, signal attenuation becomes significantly more rapid as distance increase further. The modified two-slope (TS) path loss is an extension of the OS model that accounts for the impact of different propagation environments over varying distances [26]. The formula for the modified TS path loss model is expressed as

$$PL_{ts}(d) = \begin{cases} l_0 + 10\gamma_1 \log_{10}(d), & d \le d_b, \\ l_0 + 10\gamma_1 \log_{10}(d_b) + 10\gamma_2 \log_{10}\left(\frac{d}{d_b}\right), & d > d_b, \end{cases} \tag{4}$$

where γ_1 and γ_2 are the path loss exponents for the first segment ($d \le d_b$) and the second segment ($d > d_b$), respectively, and d_b is the break point distance where the propagation environment changes.

4) Classical Multi-Wall Penetration Loss

The classical multi-wall (MWC) path loss model was introduced by adding an extra attenuation term to the general OS model, representing the losses caused by walls and floors penetrated by the direct path between the transmitter and the receiver [27]. The model is expressed as

$$PL_{mwc}(d) = PL_{os}(d) + l_c + \sum_{i=1}^{W} k_{wi} l_i, \tag{5}$$

where l_c is a constant representing the baseline attenuation, k_{wi} is the number of penetrated walls of type i, l_i is the attenuation due to a wall of type i, and W is the total number of wall types considered.

5) Shadowing Effect

The shadowing effect arises due to the presence of large obstacles, such as buildings, trees and terrain features, along the propagation path between the transmitter and receiver [28]. These obstacles partially or completely block the transmission link, causing signal power to attenuate through mechanisms such as absorption, reflection, scattering and diffraction. Unlike the path-based deterministic function used to model path loss, the shadowing effect can be considered a random variation superimposed on the existing attenuation, which quantifies the impact of varying environmental obstacle distributions between a fixed transmitter and receiver pair.

To account for the randomness, the random variable of the shadowing effect ξ_s is modeled as the log-normal distribution [29], i.e.,

$$\ln(\xi_s) \sim \mathcal{N}(\mu, \sigma^2), \tag{6}$$

and the probability density function (PDF) is given by

$$f_{\xi_s}(x_s) = \frac{1}{x_s \sigma \sqrt{2\pi}} \exp\left(-\frac{(\ln(x_s) - \mu)^2}{2\sigma^2}\right), \tag{7}$$

where x_s denotes a specific realization of the random variable ξ_s, μ is the mean of the logarithmic values, and σ is the standard deviation of the logarithmic values.

The received signal power P_r in a propagation model is typically expressed as the combination of path loss and shadowing effect, given by:

$$P_r = P_t \cdot PL(d) \cdot \xi_s, \tag{8}$$

where P_t is the transmit signal power, $PL(d)$ represents the path loss at a distance d that computed utilizing the above deterministic path loss models, $\xi_s = 10^{\frac{\xi_\sigma}{10}}$ is a shadowing factor, ξ_σ is a normal random variable with zero mean and variance σ^2. Alternatively, the expression can be written in logarithmic form as $P_r(dB) = P_t(dB) - PL(dB) + \xi_\sigma$.

B. Small-Scale Fading

Small-scale fading refers to the rapid variations in signal amplitude and phase caused by multipath propagation and Doppler effects in the propagation environment. In contrast to the random variations of shadowing effect, small-scale fading is characterized by more rapid spatial random variations in signal power. Channel models such as Rayleigh, Rician and Nakagami-m distributions are commonly used to characterize the small-scale fading in IEEE 802.11a deployments [30].

1) Multipath Fading

Multipath fading arises due to the reflection, diffraction and scattering of signals off environmental obstacles, resulting in multiple signal paths that interfere constructively or destructively at the receiver [6]. This phenomenon is typically represented by the multipath fading channel response:

$$c_{mul}(t) = \sum_{i=1}^{L_m} \alpha_i \delta(t - \tau_i), \tag{9}$$

where L_m is the total number of multipath components, α_i represents the amplitude (or path gain) of the i-th path, and τ_i denotes the time delay of the i-th path. These effects introduce delay spread and frequency-selective fading, which distort signals and degrade performance, especially in high-speed environments [31].

2) Rayleigh Fading

The Rayleigh fading is widely applied in NLoS conditions, where the received signal is the sum of multiple scattered components, each with random amplitude and phase [32], [33]. The complex channel response for Rayleigh fading is expressed as [34]

$$c_{ray}(t) = \sum_{i=-\infty}^{\infty} h_i e^{j\phi_i}, \tag{10}$$

where t is the time variable, h_i is the amplitude of the i-th multipath component, $j = \sqrt{-1}$ is the imaginary unit in complex numbers, and ϕ_i is the i-th random phase offset. Based on the polar coordinating of a complex random process, we can observe envelope and phase variations of the fading. The probability density function (PDF) of the amplitude h follows a Rayleigh distribution, which can be obtained as

$$f_{ray}(r) = \frac{r}{\Omega} e^{-\frac{r^2}{2\Omega}}, \quad r \ge 0, \tag{11}$$

where the average received signal power is given by

$$\Omega = \frac{1}{2} \sum_{i=-\infty}^{\infty} h_i^2, \tag{12}$$

These characteristics make the Rayleigh model an essential tool for evaluating IEEE 802.11a systems deployed in urban or indoor environments where signals experience extensive scattering.

3) Rician Fading

The Rician fading is used in environments where there is a dominant LoS component, capturing both the deterministic LoS signal and the random scattered components [30], [35]. The complex channel response for Rician fading is expressed as [36]

$$c_{ric}(t) = h_d e^{j\phi_d} + \sum_{i=-\infty}^{\infty} h_i e^{j\phi_i}, \tag{13}$$

where h_d is the amplitude of the direct path, ϕ_d is the phase of the direct path. Let Ω_{dir} represent the power of the LoS component and $\Omega_{rad} = \sigma^2$ be the total power of the scattered components. The Rician factor can be represented by the following power ratio:

$$K = \frac{\Omega_{dir}}{\Omega_{rad}} = \frac{h_d^2}{2\sigma^2}. \tag{14}$$

The PDF expression of the received signal amplitude h in the Rician fading is given by:

$$f_{ric}(r) = \frac{r}{\Omega_{rad}} \exp\left(-\frac{r^2}{2\Omega_{rad}} - K\right) I_0\sqrt{\left(\frac{2Kr^2}{\Omega_{rad}}\right)}, \tag{15}$$

where r is the amplitude of the received signal, $I_0(\cdot)$ is the modified Bessel function of the first kind and zero order. This model is particularly applicable in environments with a dominant LoS path along with multipath scattering, such as outdoor or suburban wireless communication systems, where a higher value of K signifies a stronger LoS component.

4) Nakagami-m Fading

The Nakagami-m model offers flexibility in modeling fading severity, making it suitable for a wide range of environments, from strong LoS to severe multipath scenarios [5], [37], [38]. The complex baseband gain $c(t)$ of the Nakagami-m channel is defined as [39]

$$c_{nak}(t) = \sqrt{2} \cdot \frac{\Gamma(m + 1/2)}{\Gamma(m)} \cdot \left(\frac{m}{\Omega}\right)^{m/2} \cdot r \tag{16}$$

where m is the fading parameter (also called the shape parameter) with $m \geq 0.5$, $\Omega = \mathbb{E}[r^2]$ represents the average power of the signal and $\Gamma(m)$ is the Gamma function. When $m = 1$, it corresponds to Rayleigh fading, and when $m > 1$, it describes a more stable channel with reduced fading. Ω represents the average received power, which is the second moment of the Nakagami-m distribution. The PDF of the signal amplitude h in the Nakagami-m fading is given by [39]

$$f_{nak}(r) = \frac{2m^m r^{2m-1}}{\Gamma(m)\Omega^m} e^{-\frac{mr^2}{\Omega}}, \quad r \geq 0, \tag{17}$$

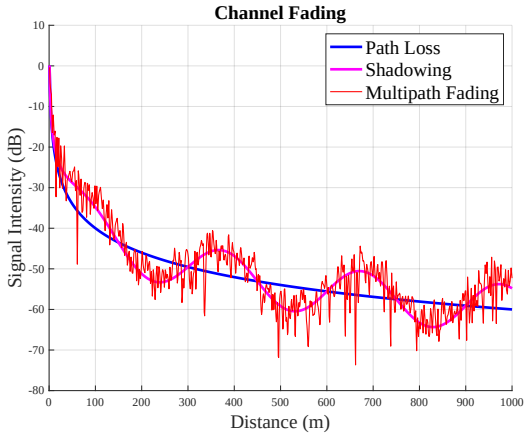

Fig. 3. Combined effects of path loss, shadowing effect and multipath fading.

This model is particularly useful for IEEE 802.11a systems operating in the 5 GHz band, effectively capturing varying fading conditions in environments like indoor office spaces and outdoor urban settings.

5) Doppler Effect

In 802.11 networks, the Doppler shift leads to signal distortion, reduced throughput and increased error rates, especially in high-speed scenarios [40]–[42]. Doppler frequency shift occurs when the relative motion between the transmitter and receiver which leads to either a frequency increase or decrease depending on the direction of motion. This is a critical issue in high-speed scenarios, such as vehicular or aerial networks.

This Doppler effect can be multiplicatively superimposed on the channel response, leading to the stretching or compression of the signal spectrum [43]. For example, a Rician channel with the superimposed Doppler effect can be expressed as [44]

$$c_{dop}(t) = \sum_{i=-\infty}^{\infty} h_i e^{j2\pi t f_D \cos\theta_i + j\phi_i}, \tag{18}$$

$$c_{dop}(t) = h_d e^{j2\pi t f_D \cos\theta_d + j\phi_d} + \sum_{i=-\infty}^{\infty} h_i e^{j2\pi t f_D \cos\theta_i + j\phi_i}, \tag{19}$$

where the term $f_D \cos\theta_d$ and $f_D \cos\theta_i$ denote the Doppler frequency offset with respect to the motion of the mobile unit, θ_d and θ_i are the angles of arrival (AoAs) at the direct path and the i-th multipath, respectively. where f_D represents the maximum Doppler frequency shift and is calculated as

$$f_D = \frac{v_{t,r}}{v_0} \cdot f_0, \tag{20}$$

where $v_{t,r}$ is the relative velocity between the transmitter and receiver, v_0 is the speed of light and f_0 is the transmitted signal frequency. The power spectral density (PSD) of the Jakes Doppler spectrum is used to model the Doppler spread in wireless channels. The formula is given as

$$S_D(f) = \frac{1}{\pi f_D \sqrt{1 - \left(\frac{f}{f_D}\right)^2}}, \quad |f| \leq f_D \tag{21}$$

TABLE I
COMPARISON OF PATH LOSS, SHADOWING, AND SMALL-SCALE FADING CHARACTERISTICS

Attributes	**Path Loss**	**Shadowing**	**Small-Scale Fading**
Attenuation	Large	Medium	Small
Variation	Fixed	Random	Random
Distribution	Deterministic Function	Log-normal	Rayleigh or Rician
Range of Effect	10 m $\sim$ 10000 m	20 m $\sim$ 200 m	1 cm $\sim$ 10 m

This model applies to $|f| \leq f_D$, where the power spectral density follows an inverted semi-elliptical distribution, with lower power density near the maximum Doppler shift.

Finally, we illustrate the combined effects of path loss, shadowing, and small-scale multipath in Fig. 3. It is evident from the figure that the magnitude of path loss is a deterministic function that attenuates with increasing distance, whereas shadowing and small-scale fading introduce superimposed random perturbations. Specifically, path loss exhibits slower variations, while shadowing and small-scale fading occur at faster rates [29]. Furthermore, we provide a comparison of the characteristics of path loss, shadowing, and small-scale fading in Table I.

IV. ADDITIVE INTERFERENCE

Additive interference refers to disturbances that are directly superimposed on the received signal during propagation. The primary sources of additive interference are inherent physical phenomena within the propagation environment or communication system, which persist regardless of whether a signal is being transmitted. Detailed descriptions of the additive interference are provided in the following subsections.

A. Thermal Noise

Thermal noise in wireless channels is attributed to the natural thermal energy present in the propagation medium of electromagnetic waves. As electromagnetic waves travel through the atmosphere, the thermal agitation of charged particles, such as electrons, ions and molecules, within the medium introduces random fluctuations in the electric field. This type of random, continuous fluctuation with a stable power spectral density is modeled as standard AWGN [45], [46], i.e.,

$$w_{tem}(t) \sim \mathcal{N}(0, P_{tem}), \tag{22}$$

which is superimposed on the received signal as a persistent background noise. The variance P_{tem} of the noise is directly related to the total thermal noise power, which is determined by the Nyquist formula:

$$P_{tem} = k \cdot T \cdot B, \tag{23}$$

where k is the Boltzmann constant, equal to 1.38×10^{-23} J/K, T is the absolute temperature in kelvin (K) and B is the system bandwidth in hertz (Hz).

Thermal noise reduces SNR of the communication system, thereby reducing the clarity of the transmitted signal and increasing the bit error rate [47]. Since the kinetic energy of these particles depends on temperature and bandwidth, the effect of thermal noise is particularly pronounced in high-frequency systems, where higher bandwidth and temperature exacerbate the reduced transmission performance [48].

B. Adjacent Channel Interference

Adjacent channel interference (ACI) in the context of IEEE 802.11a systems arises when power from adjacent frequency channels leaks into the desired communication channel. This leakage occurs typically due to imperfections in the limited channel isolation, non-ideal filtering and partial overlap of spectrum, although the signal subcarriers are orthogonal in 802.11a systems [33]. The primary result of ACI is signal distortion, which degrades the overall signal quality [49]. This effect is especially problematic in densely packed frequency bands, as signals from neighboring channels overlap, causing further degradation and an increase in error rates. The ACI at a given terminal can be represented as [8], [9], [50], [51]:

$$w_{aci} = \sum_{i=1}^{m} \left(\frac{P_{IB}}{\eta} + P_{OOB} \right) \cdot PL_{os}(d) \cdot \xi_i, \tag{24}$$

where m is the number of interference sources, η is the adjacent channel selectivity of a desired terminal, P_{IB} and P_{OOB} are the in-block and out-of-block power, and ξ_i is an identical lognormal random variable for shadowing. The random variable of ACI follows the weighted log-normal PDF [52]:

$$f_{aci}(x) = \sum_{i=1}^{N} w_i \cdot \frac{1}{x \cdot \sqrt{2\pi\sigma_i^2}} \exp\left(-\frac{(\ln x - \mu_i)^2}{2\sigma_i^2} \right), \tag{25}$$

where x is the received interference signal power, N is the number of log-normal distributions, μ_i and σ_i are the mean and standard deviation of the i-th log-normal distribution, w_i is the weight of the i-th log-normal distribution satisfying $\sum_{i=1}^{N} w_i = 1$.

C. Co-Channel Interference

Co-channel interference (CCI) refers to the interference caused by the overlap of multiple signals under spectrum reuse and is a common type of interference in cellular and WLAN systems [50], [53]. It arises due to the uncertainty in the number and spatial distribution of communication nodes, as well as the imperfections in spectrum sensing mechanisms [54]–[57]. As a result, a single receiver inevitably receives co-channel interference signals from multiple unintended transmitters operating in the same frequency band. The severity of CCI is influenced by several factors, including the power

of the interfering signals and the density of the transmitter distribution [58]. Let I and J are the total numbers of disjoint regions along the angle and radius axes, the total CCI at the receiver can be expressed as the sum of interference contributions from all spatial regions:

$$w_{cci}(t) = \sum_{i=1}^{I}\sum_{j=1}^{J} s_{ij}(t) \cdot g_{ij}(t) \cdot PL(t) \cdot 10^{\frac{\xi_\sigma}{10}}, \tag{26}$$

where the signal power of the interference node in region (i, j) can be represented by

$$s_{ij}(t) = P_{ij} e^{-\alpha d_{e,ij}}, \tag{27}$$

where P_{ij} is the transmit power of the interference node, α is the attenuation factor that models the exponential decay of the signal with distance, $d_{e,ij}$ is the Euclidean distance between the interference node and the receiver, $PL(t)$ is the path loss function of distance, and the shadowing effect ξ_σ is a normally distributed random variable with mean zero and variance σ^2. The indicator function $g_{ij}(t)$ is given by

$$g_{ij}(t) = \begin{cases} 1, & \text{if the interference transmits a signal,} \\ 0, & \text{otherwise,} \end{cases} \tag{28}$$

where $g_{ij}(t)$ takes the value of 1 if an interference node in region (i, j) transmits a signal and 0 if no interference occurs from that region.

In 802.11 networks, CCI significantly impacts the throughput of the system, particularly in high-density environments where multiple access points (APs) share the same frequency bands. Insufficient isolation between transmitters results in severe throughput degradation, as multiple signals from different transmitters interfere with each other, causing data collisions and retransmissions. The resulting interference leads to a reduction in the effective data rate and an increase in packet loss [59].

D. Inter-Symbol Interference

Inter-Symbol Interference (ISI) occurs when multiple symbols transmitted over a communication channel overlap with each other due to the dispersive nature of the channel [60]–[64]. This interference is caused by factors such as multi-path propagation, limited channel bandwidth and filter mismatch. ISI results in the distortion of the received signal, thereby reducing the system's bit error rate (BER) performance. The mathematical model for the received signal in the presence of ISI can be expressed as

$$w_{isi}(t) = \sum_{k=1}^{K} x_k \, c(t - kT), \tag{29}$$

where K is the total transmit time, x_k is the transmitted symbol at time kT, $c(t)$ is the impulse response of the channel and T is the symbol duration.

For simplicity, we consider only the impact of the previous and next symbols on the current symbol. The received signal $y(t)$ can be written as

$$y(t) = x_0 c(t) + x_{-1}\, c(t + T) + x_{+1} c(t - T), \tag{30}$$

where $x_0\, c(t)$ is the desired component from the current symbol, $x_{-1}\, h(t+T)$ represents ISI from the previous symbol, $x_{+1}\, h(t - T)$ denotes ISI from the next symbol.

E. Electromagnetic Interference

Electromagnetic Interference (EMI) arises from external electromagnetic sources unrelated to the communication system, such as industrial equipment, power lines, or other wireless communication devices [65], [66]. These sources generate unintended electromagnetic fields that interfere with wireless communication systems by introducing distortions or noise into the communication channel. EMI typically exhibits varying frequency characteristics and amplitude depending on the source, which can be modeled as [67]

$$w_{emi} = \sum_{i=1}^{N} h_i(t) \cdot e^{-j2\pi \cdot f_{emi} \cdot t + \phi_i}, \tag{31}$$

where the parameter $h_i(t)$ represents the path gain for the ith interference path, accounting for the propagation properties of each path. The term f_{emi} denotes the central frequency of the interfering electromagnetic signal, which determines the spectral characteristics of the EMI. The parameter ϕ_i represents the phase shift of the ith path, modeled as a uniformly distributed random variable to reflect the randomness of the phase changes. The number of paths N depends on the environmental factors such as reflections, diffractions and scatterings within the wireless channel. In the presence of the additive interference EMI, the received signal $y(t)$ is represented as [68]

$$y(t) = c(t) \cdot x(t) + w_{emi}, \tag{32}$$

where $c(t)$ is the gain for the desired signal path, $x(t)$ is the transmitted signal.

V. Impact of the Interference on Signal Characteristics

The impact of interference can be quantified as a complex-valued gain, which characterizes channel state information by introducing random variations in signal amplitude, phase, frequency, and time components. To evaluate the impact, in this section, we first model the propagation signal on the I-Q plane as shown in Fig. 4. Then, we analyze how additive and multiplicative interference affect the key signal characteristics.

A. Propagation Signal Representation

Without loss of generality, the transmitted signal $x(t)$ can be represented as a complex signal:

$$x(t) = I_x + jQ_x = h_x e^{j\phi_x}, \tag{33}$$

where I_x and Q_x are the in-phase and quadrature components of the signal, h_x is the amplitude, and ϕ_x is the phase. The amplitude and phase are given by

$$h_x = \sqrt{I_x^2 + Q_x^2}, \quad \phi_x = \tan^{-1}\left(\frac{Q_x}{I_x}\right). \tag{34}$$

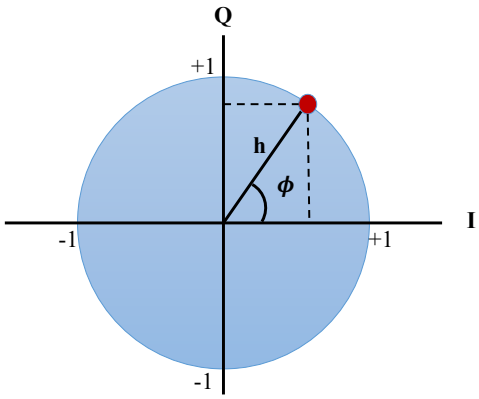

Fig. 4. The mapping of the original signal on the I-Q plane.

To model the multiplicative interference, we consider the channel gain $c(t)$ as a time-varying random process that directly multiplies the transmitted signal. Thus, the received signal $y(t)$ under the influence of the multiplicative interference can be expressed as

$$y(t) = c(t)x(t), \tag{35}$$

where $c(t)$ is a complex-valued random variable, which can be decomposed as

$$c(t) = h_c(t)e^{j\theta_c(t)}, \tag{36}$$

where $h_c(t)$ denotes the amplitude fluctuation caused by large-scale fading, shadowing, or fast fading, and $\theta_c(t)$ represents the phase fluctuation induced by random phase shifts from multipath propagation or Doppler effects. Therefore, the received signal can be rewritten as

$$y(t) = h_c(t)e^{j\theta_c(t)}x(t) = h_c(t) \cdot h_x \cdot e^{j(\phi+\theta_c(t))}. \tag{37}$$

For analysis purposes, $h_c(t)$ is typically modeled as a Rician or Rayleigh random variable, and $\theta_c(t)$ is often modeled as a uniform random variable on $[0, 2\pi)$.

The additive interference $w(t)$ can be also represented as a complex noise with two components:

$$w(t) = I_w + jQ_w, \tag{38}$$

where I_w and Q_w are the in-phase and quadrature components of the additive interference, which are independent Gaussian random variables with zero mean and variance σ^2, i.e., $I_w, Q_w \sim \mathcal{N}(0, \sigma^2)$. The received signal $y(t)$ under the influence of noise can be written as

$$y(t) = x(t) + w(t) = (I_x + I_w) + j(Q_x + Q_w). \tag{39}$$

This equation shows that the noise shifts the position of the original signal $x(t)$ on the I-Q plane by (I_w, Q_w), which affects its amplitude, phase, frequency and time delay.

B. Impact of the Multiplicative Interference

1) Amplitude

The amplitude h' of the received signal $y(t)$ is affected by the channel gain $c(t)$. If the transmitted signal has amplitude h, then the amplitude of the received signal becomes:

$$h' = |h_{\text{large}}(t)\, h_{\text{small}}(t)| \cdot h_x. \tag{40}$$

The large-scale fading component $h_{\text{large}}(t)$ can be modeled as

$$h_{\text{large}}(t) = \frac{1}{d^n} \cdot 10^{\frac{X_\sigma}{10}}, \tag{41}$$

where d is the distance between the transmitter and receiver, n is the path loss exponent and X_σ is a Gaussian random variable representing shadowing. The small-scale fading component $h_{\text{small}}(t)$ is often modeled as Rayleigh or Rician distributed, depending on the presence of a LoS path. This causes random variations in amplitude, leading to deep fades that affect the quality of the received signal.

2) Phase

The phase ϕ of the received signal $y(t)$ is altered by the phase component of the channel gain $c(t)$. If $c(t) = |h_c(t)|e^{j\theta_c(t)}$, the received signal becomes:

$$y(t) = |h_c(t)|\, e^{j\theta_c(t)}\, x(t) = h_x\, |h_c(t)|\, e^{j(\phi_x+\theta_c(t))}. \tag{42}$$

The phase shift $\Delta\phi$ introduced by the channel can be expressed as

$$\phi' = \phi_x + \theta_c(t), \tag{43}$$

$$\Delta\phi = \theta_c(t). \tag{44}$$

This phase shift depends on the multipath components, as each path may introduce a different delay and phase shift. In Rayleigh fading, $\theta_c(t)$ is uniformly distributed between $[0, 2\pi]$, leading to random changes in the signal's phase. For phase-modulated systems (like QPSK), this phase shift can cause errors in the demodulation process.

3) Frequency

The impact of multiplicative interference on signal frequency is primarily caused by Doppler shift. The frequency shift $\Delta f = \frac{v_{t,r}}{v_0} \cdot f_0$ is caused by the relative movement between the transmitter and receiver. The transmitted signal is represented as

$$x(t) = h_x \cos(2\pi f_0 t + \phi_x), \tag{45}$$

and the received signal under multiplicative interference can be given by

$$y(t) = h_x \cos\left(2\pi(f_0 + \Delta f)t + \phi_x\right). \tag{46}$$

The frequency offset f_0 shifts the carrier frequency, causing frequency errors that affect synchronization and symbol detection. These errors are significant in high-mobility scenarios, such as vehicles or mobile devices in motion.

4) Time Delay

Time delay is caused by multipath propagation, where each path introduces a different delay τ_i. The received signal is the superposition of multiple delayed copies of the original signal:

$$y(t) = \sum_{i=1}^{L_m} h_i\, x(t - \tau_i), \tag{47}$$

where L_m is the number of multipath components, h_i is the amplitude of the i-th path and τ_i is its corresponding delay. These delays cause ISI, which occurs when delayed copies of previous symbols interfere with the current symbol. The total delay spread is defined as the difference between the arrival times of the earliest and latest paths. Delay spread is a major factor in determining the cyclic prefix length in OFDM systems.

C. Impact of the Additive Interference

1) Amplitude

The amplitude h of the received signal $y(t)$ is the distance from the origin to the point $(I_x + I_w, Q_x + Q_w)$ in the I-Q plane and it can be calculated as

$$h' = \sqrt{(I_x + I_w)^2 + (Q_x + Q_w)^2}. \tag{48}$$

If the noise is small relative to the signal, we can expand the amplitude using a first-order Taylor approximation. The change in amplitude Δh can be approximated as

$$\Delta h = h' - h_x \approx \frac{I_x\, I_w + Q_x\, Q_w}{\sqrt{I_x^2 + Q_x^2}}, \tag{49}$$

where $h_x = \sqrt{I_x^2 + Q_x^2}$ is the original amplitude. This formula indicates that the change in amplitude depends linearly on the noise components I_w and Q_w. Geometrically, this means that the star points in the I-Q plane will "move" away from their ideal positions and in amplitude modulation (AM) systems, this can lead to misinterpretation of the signal.

2) Phase

The phase ϕ of a signal is the angle between the I-axis and the vector connecting the origin to the point $(I_x + I_w, Q_x + Q_w)$. The phase ϕ of the received signal $y(t)$ is given by:

$$\phi' = \tan^{-1}\left(\frac{Q_x + Q_w}{I_x + I_w}\right). \tag{50}$$

The change in phase $\Delta\phi$ caused by noise can be approximated using a first-order Taylor expansion around (I, Q) as

$$\Delta\phi = \phi' - \phi_x \approx \frac{Q_w\, I_x - I_w\, Q_x}{I_x^2 + Q_x^2}. \tag{51}$$

This formula indicates that the phase shift is influenced by both the in-phase noise I_w and the quadrature noise Q_w. In the I-Q plane, this means the position of the star points will rotate around the origin. For systems like Phase Shift Keying (PSK), which rely on phase detection, even a small change in phase can cause errors in symbol detection, leading to an increased BER.

3) Frequency

Although additive interference does not directly alter the carrier frequency f_0, it indirectly impacts the frequency estimation of IEEE 802.11a OFDM systems, resulting in carrier frequency offset (CFO). The transmitted signal can be modeled as

$$x(t) = h_x \cos(2\pi f_x t + \phi_x), \tag{52}$$

and the received signal under multiplicative interference can be given by

$$y(t) = h_x \cos\left(2\pi(f_x + \Delta f)t + \phi_x\right) + w_f(t), \tag{53}$$

where the noise $w_f(t)$ introduces randomness in the frequency estimation process. Due to the fact that frequency is the time derivative of phase:

$$f = \frac{d\phi}{dt}, \tag{54}$$

the accumulated phase error can introduce a frequency error in the time domain. The relationship between phase disturbance, phase rate error, and frequency error can be expressed as:

$$\Delta\phi(t) \implies \Delta\dot{\phi}(t) \implies \Delta f. \tag{55}$$

If a frequency tracking system, such as a PLL, is used to estimate the frequency, the additive interference will introduce errors in the phase estimate, which indirectly results in frequency errors. This leads to frequency jitter in systems like Frequency Shift Keying (FSK). The frequency error Δf can be modeled as a zero-mean Gaussian random variable whose variance is proportional to SNR. The variance of frequency error σ_f^2 can be approximated as

$$\sigma_f^2 \approx \frac{1}{SNR \cdot T_{obs}}, \tag{56}$$

where T_{obs} is the observation time and SNR is the signal-to-noise ratio.

4) Time Delay

Time delay is a critical parameter in time-of-arrival (TOA) and time-difference-of-arrival (TDOA) positioning systems. The received signal with time delay τ is modeled as

$$y(t) = x(t - \tau) + w(t). \tag{57}$$

If the additive interference $w(t)$ is present, it affects the detection of the signal's arrival time. Positioning systems typically use cross-correlation methods to estimate the time delay τ. The cross-correlation function $R(\tau)$ between the transmitted signal $x(t)$ and received signal $y(t)$ is given by:

$$R(\tau) = \int x(t)\, y(t + \tau)\, dt. \tag{58}$$

The position τ_y of the peak of $R(\tau)$ indicates the time delay. However, when noise $w(t)$ is present, the peak location of the cross-correlation may shift, leading to an estimation error $\Delta\tau$. This error can be approximated as

$$\Delta\tau \approx \frac{w(t)}{\partial_t R(\tau)}, \tag{59}$$

where $\partial_t R(\tau)$ is the time derivative of the cross-correlation function. The precision of time delay estimation depends on SNR. Higher SNR leads to smaller errors in delay estimation, while lower SNR increases the delay variance.

VI. Challenges and Future Research Directions

A. Challenges

1) Dynamic and Complex Channel Molding

Wireless channels are inherently dynamic and are influenced by various interference sources, including multipath propagation, Doppler effects, and environmental changes. These characteristics introduce significant challenges in accurately modeling channel behavior. In urban and public environment, overlapping signals and user mobility further deteriorate the complexity of channel modeling [69]. Traditional channel models struggle to address these challenges effectively. Advanced geometric and stochastic models are required to capture the intricate behavior of dense network environments and provide accurate predictions of channel behavior [70].

2) Real-Time Interference Suppression

Due to rapidly changing channel conditions and high mobility, there are additional complexity introduced in dynamic communication scenarios, such as vehicular, mobile users and drone networks [71]. Real-time suppression of intercarrier interference is one of the primary challenges in these scenarios. Techniques such as reinforcement learning and adaptive filtering have shown promising potential for interference suppression. However, their high computational complexity poses significant challenges for large-scale deployment [72]. To address this issue, it is essential to design flexible and adaptive algorithms that achieve a balance between interference characterization and latency requirements.

3) Interference Analysis and SNR Degradation

Additive interference plays a critical role in degrading the SNR in IEEE 802.11a systems, directly affecting signal quality and throughput [73]. The Gaussian approximation of intercarrier interference has proven effective in estimating error probabilities under fading conditions [74]. However, as noise levels increase, the accuracy of these approximations diminishes, leaving room for improvement in interference estimating techniques. Furthermore, in high-density environments, the coexistence of CCI and ACI exacerbates the issue, demanding advanced mitigation strategies.

B. Future Research Directions

1) Advanced Channel Modeling

The machine learning-based channel modeling can significantly enhance the performance of adaptive communication systems by providing real-time insights into channel dynamics. Moreover, advanced geometric modeling captures spatial propagation characteristics, while stochastic modeling better represents random channel behaviors. Combining these two approaches can effectively improve modeling accuracy and enhance the representation of complex channel dynamics. Additionally, layered channel modeling that integrates different large-scale and small-scale channel characteristics offers a practical approach to adapt to complex network environments.

2) Emerging Technologies Integration

The integration of IEEE 802.11a systems with emerging technologies such as reconfigurable intelligent surfaces (RIS) and terahertz communication offers new opportunities for interference suppression and channel reconfiguration. These technologies enable dynamic control of the wireless environment, allowing for improved signal quality and reduced interference. To further suppress interference, developing efficient adaptive algorithms that balance interference characterization and latency optimization is essential. Additionally, distributed interference management frameworks can be implemented in large-scale networks, leveraging collaborative node management and physical layer technology to minimize interference and enhance overall network efficiency.

3) Cross-Layer Optimization

Based on the interference analysis, cross-layer optimization integrates physical, MAC, and application layers to address SNR degradation and secure communication, fully leveraging the capabilities of IEEE 802.11a systems. At the physical layer, techniques such as secure beamforming, channel coding, and source coding are essential for mitigating interference and improving signal reliability. The MAC layer further enhances these efforts through dynamic spectrum allocation, time-slot scheduling, and power control, ensuring efficient resource utilization and minimizing interference. While these techniques focus on improving SNR, cryptographic encryption in the application layer plays a complementary role by safeguarding transmitted data and enhancing overall communication security. As a result, the coordinated design of these technologies across layers enables robust interference suppression, improved SNR, and secure communication in dynamic and high-interference environments.

VII. Conclusion

In this paper, we provided a comprehensive review of channel modeling and interference mechanisms in IEEE 802.11a wireless communication systems. Based on different interference sources, we categorized existing interference into two multiplicative interference and additive interference. Specifically, we first analyzed the characteristics of multiplicative interference, which includes large-scale fading caused by path loss and shadowing, as well as small-scale fading induced by multipath propagation and Doppler effects. We then examined additive interference, which was further classified into thermal noise, ACI, CCI and EMI. For each type of interference, we analyzed its impact on critical signal characteristics, including amplitude, phase, frequency, and time delay. Some future research directions were also suggested in this paper to address key challenges, such as multi-source interference coexistence, dynamic interference prediction, and adaptive channel modeling. This paper will provide valuable references for research on backward compatibility of legacy IEEE 802.11a wireless communication systems in modern networks.

References

[1] J. G. Andrews and et al., "What will 5G be?" *IEEE J. Sel. Areas Commun.*, vol. 32, no. 6, pp. 1065–1082, Jun. 2014.

[2] X. Chen, M. Liu, and T. Yang, "Hybrid statistical and machine learning channel models for WLAN optimization," *IEEE Commun. Lett.*, vol. 27, no. 2, pp. 467–471, Feb. 2023.

[3] G. Bianchi, "Performance analysis of the IEEE 802.11 distributed coordination function," *IEEE J. Sel. Areas Commun.*, vol. 18, no. 3, pp. 535–547, Mar. 2000.

[4] E. Perahia and R. Stacey, *Next generation wireless LANs: 802.11 n and 802.11 ac*. U.K.: Cambridge Univ. Press, 2013.

[5] M. A. Hussein, "Performance study of IEEE 802.11 a wlan physical layer under nakagami-rice fading channel," in *Proc. Information Technology conference, the University of Technology, Baghdad*, 2009.

[6] K. Yip, T. Ng, and Y. C. Wu, "Impacts of multipath fading on the timing synchronization of IEEE 802.11a wireless LANs," in *Proc. IEEE International Conference on Communications (ICC)*, vol. 1, Apr. 2002, pp. 517–521.

[7] N. Giradkar, G. M. Asutkar, and A. Maidamwar, "OFDM based phy performance of IEEE 802.11a using various practical channel models," in *Proc. IEEE International Conference on Wireless Networks (ICWN)*. IEEE, Sep. 2010.

[8] V. Angelakis, S. Papadakis, V. Siris, and A. Traganitis, "Adjacent channel interference in 802.11a is harmful: Testbed validation of a simple quantification model," *IEEE Commun. Mag.*, vol. 49, no. 5, pp. 160–167, May 2011.

[9] C.-M. Cheng, P.-H. Hsiao, H. Kung, and D. Vlah, "Wsn07-1: Adjacent channel interference in dual-radio 802.11 a nodes and its impact on multi-hop networking," in *Proc. IEEE Global Communications Conference (GLOBECOM)*. IEEE, May 2006, pp. 1–6.

[10] D. K. Borah, R. Jana, and A. Stamoulis, "Performance evaluation of IEEE 802.11 a wireless lans in the presence of ultra-wideband interference," in *Proc. IEEE Wireless Communications and Networking (WCNC)*, vol. 1. IEEE, 2003, pp. 83–87.

[11] A. Mehbodniya and S. Aissa, "Performance analysis of a 802.11 a OFDM system in the presence of UWB and multipath interference," in *Proc. IEEE Sarnoff Symposium*. IEEE, 2007, pp. 1–5.

[12] B. Firoozbakhsh, T. G. Pratt, and N. Jayant, "Analysis of IEEE 802.11 a interference on UWB systems," in *IEEE Conference on Ultra Wideband Systems and Technologies*. IEEE, 2003, pp. 473–477.

[13] T. Wang, J. G. Proakis, E. Masry, and J. R. Zeidler, "Performance degradation of OFDM systems due to doppler spreading," *IEEE Trans. Wireless Commun.*, vol. 5, no. 6, pp. 1422–1432, Jun. 2006.

[14] M. Braun, M. Fuhr, and F. K. Jondral, "Spectral estimation-based OFDM radar algorithms for IEEE 802.11a signals," in *Proc. IEEE Vehicular Technology Conference (VTC Fall)*. IEEE, May 2012, pp. 1–5.

[15] J. B. Andersen, T. S. Rappaport, and S. Yoshida, "Propagation measurements and models for wireless communications channels," *IEEE Commun. Mag.*, vol. 33, no. 1, pp. 42–49, Jan. 1995.

[16] N. Shinohara, *Wireless power transfer via radiowaves*. John Wiley & Sons Press, 2014.

[17] D. Middleton, "Statistical-physical models of electromagnetic interference," *IEEE Trans. Electromagn. Compat.*, vol. EMC-19, pp. 106–127, May 1977.

[18] R. Zabihi and R. G. Vaughan, "Diffraction: A critical propagation mechanism," in *Proc. IEEE Canadian Conference on Electrical and Computer Engineering (CCECE)*. IEEE, 2016, pp. 1–4.

[19] T. K. Sarkar, Z. Ji, K. Kim, A. Medouri, and M. Salazar-Palma, "A survey of various propagation models for mobile communication," *IEEE Antennas Propag. Mag.*, vol. 45, no. 3, pp. 51–82, Jun. 2003.

[20] J.-H. Kim and S.-J. Oh, "Geometric optics-based propagation prediction model for wireless communications," *IEEE Wirel. Commun. Lett.*, vol. 5, no. 3, pp. 300–303, Jun. 2016.

[21] L. Possenti, M. Barbiroli, E. M. Vitucci, F. Fuschini, M. Fosci, and V. Degli-Esposti, "A study on mm-wave propagation in and around buildings," *IEEE Open J. Antennas Propag.*, vol. 4, pp. 1–12, Jul. 2023.

[22] L. G. Guimarães and E. Sampaio, "A note on snell laws for electromagnetic plane waves in lossy media," *J. Quant. Spectrosc. Radiat. Transf.*, vol. 109, no. 12, pp. 2124–2140, Dec. 2008.

[23] P. Moravek, D. Komosny, M. Simek, M. Jelinek, D. Girbau, and A. Lazaro, "Investigation of radio channel uncertainty in distance estimation in wireless sensor networks," *Telecommun. Syst.*, vol. 52, no. 3, pp. 1549–1558, Mar. 2013.

[24] S. Vougioukas, H. Anastassiu, C. Regen, and M. Zude, "Influence of foliage on radio path losses (pls) for wireless sensor network (wsn) planning in orchards," *Biosyst. Eng.*, vol. 114, no. 4, pp. 454–465, Apr. 2013.

[25] Z. Gao, W. Li, Y. Zhu, Y. Tian, F. Pang, W. Cao, and J. Ni, "Wireless channel propagation characteristics and modeling research in rice field sensor networks," *Sensors*, vol. 18, no. 9, p. 3116, Sep. 2018.

[26] D. Wang, L. Song, X. Kong, and Z. Zhang, "Near-ground path loss measurements and modeling for wireless sensor networks at 2.4 ghz," *Int. J. Distrib. Sens. Netw.*, vol. 8, no. 8, pp. 1018–1020, 2012.

[27] F. Capulli, C. Monti, M. Vari, and F. Mazzenga, "Path loss models for IEEE 802.11 a wireless local area networks," in *Proc. IEEE International Symposium on Wireless Communication Systems (ISWCS)*, 2006, pp. 621–624.

[28] M. Wildemeersch, T. Q. S. Quek, M. Kountouris, A. Rabbachin, and C. Slump, "Successive interference cancellation in heterogeneous networks," *IEEE Trans. Commun.*, vol. 62, pp. 4440–4453, Dec. 2014.

[29] B. H. Liu, B. Otis, S. Challa, P. Axon, C. T. Chou, and S. Jha, "On the fading and shadowing effects for wireless sensor networks," in *Proc. IEEE International Conference on Mobile Ad Hoc and Sensor Systems (MASS)*, 2006, pp. 51–60.

[30] Z. Hadzi-Velkov and B. Spasenovski, "On the capacity of IEEE 802.11 dcf with capture in multipath-faded channels," *Int. J. Wirel. Inf. Netw.*, vol. 9, pp. 191–199, Jun. 2002.

[31] T. V. Nguyen, D. N. Nguyen, M. D. Renzo, and R. Zhang, "Leveraging secondary reflections and mitigating interference in multi-IRS/RIS aided wireless networks," *IEEE Trans. Wireless Commun.*, vol. 22, pp. 502–517, Jan. 2021.

[32] T. S. Rappaport, *Wireless communications: principles and practice*. U.K.: Cambridge Univ. Press, 2024.

[33] G. Santella and F. Mazzenga, "A hybrid analytical-simulation procedure for performance evaluation in M-QAM-OFDM schemes in presence of nonlinear distortions," *IEEE Trans. Veh. Technol.*, vol. 47, no. 1, pp. 142–151, Feb. 1998.

[34] F. Daneshgaran, M. Laddomada, F. Mesiti, and M. Mondin, "Saturation throughput analysis of IEEE 802.11 in the presence of non-ideal transmission channel and capture effects," *IEEE Trans. Wireless Commun.*, vol. 7, pp. 1276–1286, Jun. 2007.

[35] M. M. Carvalho and J. J. Garcia-Luna-Aceves, "Modeling single-hop wireless networks under rician fading channels," in *Proc. IEEE Wireless Communications and Networking Conference (WCNC)*, vol. 1, 2004, pp. 219–224.

[36] K. Yip, Y.-C. Wu, and T. Ng, "Timing-synchronization analysis for IEEE 802.11a wireless LANs in frequency-nonselective rician fading environments," *IEEE Trans. Wireless Commun.*, vol. 3, pp. 387–394, Apr. 2004.

[37] A. Goldsmith, *Wireless Communications*. U.K.: Cambridge Univ. Press, 2005.

[38] T. S. Rappaport, S. Sun, R. Mayzus, Y. Azar, K. Wang, G. N. Wong, J. K. Schulz, M. K. Samimi, and F. Gutierrez, "Small-scale and local area transitional characteristics of millimeter-wave propagation," *IEEE Trans. Antennas Propag.*, vol. 65, no. 12, pp. 6474–6490, Dec. 2017.

[39] L.-C. Wang, W.-C. Liu, A. Chen, and K.-N. Yen, "Joint rate and power adaptation for wireless local area networks in generalized nakagami fading channels," *IEEE Trans. Veh. Technol.*, vol. 58, pp. 1375–1386, Mar. 2009.

[40] P. Robertson and S. Kaiser, "The effects of doppler spreads in OFDM (a) mobile radio systems," in *Proc. IEEE VTS 50th Vehicular Technology Conference*, vol. 1, 1999, pp. 329–333.

[41] T. Zemen, L. Bernadó, N. Czink, and A. Molisch, "Iterative time-variant channel estimation for 802.11p using generalized discrete prolate spheroidal sequences," *IEEE Trans. Veh. Technol.*, vol. 61, pp. 1222–1233, Mar. 2012.

[42] L. Cheng, B. Henty, R. L. Cooper, D. Stancil, and F. Bai, "A measurement study of time-scaled 802.11a waveforms over the mobile-to-mobile vehicular channel at 5.9 ghz," *IEEE Commun. Mag.*, vol. 46, pp. 92–99, Jun. 2008.

[43] A. E. Gebali and R. Landry, "Multi-frequency interference detection and mitigation using multiple adaptive iir notch filter with lattice structure," *J. Comput. Commun.*, May 2021.

[44] T. Luo, Z. Wen, J. Y. Li, and H.-H. Chen, "Saturation throughput analysis of wave networks in doppler spread scenarios," *IET Commun.*, vol. 4, pp. 817–825, Aug. 2010.

[45] K. Segall, D. Schult, U. Ray, and T. K. Ohsumi, "Numerical simulation of thermal noise in josephson circuits," *arXiv: Superconduct.*, 2011.

[46] T. Meng, B. McFarland, D. Su, and J. Thomson, "Design and implementation of an all-cmos 802.11a wireless lan chipset," *IEEE Commun. Mag.*, vol. 41, pp. 160–168, Oct. 2003.

[47] H. Kang, J. Kwak, T. Pratt, and G. L. Stüber, "Analytical framework for optimal combining with arbitrary-power interferers and thermal noise," *IEEE Trans. Veh. Technol.*, vol. 57, pp. 1564–1575, Jul. 2008.

[48] F. Jondral, "White gaussian noise – models for engineers," *Frequenz*, vol. 72, pp. 293–299, Jul. 2018.

[49] J. Seo, S.-J. Cho, and K. Feher, "Impact of non-gaussian impulsive noise on the performance of high-level QAM," *IEEE Trans. Electromagn. Compat.*, vol. 31, pp. 177–180, Aug. 1989.

[50] W. Gosling, "A simple mathematical model of co-channel and adjacent channel interference in land mobile radio," *IEEE Trans. Veh. Technol.*, vol. 29, no. 4, pp. 361–364, Nov. 1980.

[51] V. Angelakis, S. Papadakis, V. A. Siris, and A. Traganitis, "Adjacent channel interference in 802.11 a is harmful: Testbed validation of a simple quantification model," *IEEE Communications Magazine*, vol. 49, no. 3, pp. 160–166, 2011.

[52] M. Kim, Y. Han, Y. Yoon, Y.-J. Chong, and H. Lee, "Modeling of adjacent channel interference in heterogeneous wireless networks," *IEEE Commun. Lett.*, vol. 17, no. 9, pp. 1774–1777, 2013.

[53] J. Li, S. Li, F. Zhao, and R. Du, "Co-channel interference modeling in cognitive wireless networks," *IEEE Trans. Commun.*, vol. 62, no. 9, pp. 3114–3128, Sep. 2014.

[54] L.-C. Wang and C. Lea, "Co-channel interference analysis of shadowed rician channels," *IEEE Commun. Lett.*, vol. 2, no. 3, pp. 67–69, Mar. 1998.

[55] M. Kocaturk and S. Gupta, "Simulation of co-channel interference in coexisting cellular tdma networks," *IEEE Trans. Veh. Technol.*, vol. 43, no. 4, pp. 753–761, Nov. 1994.

[56] X. Ge, K. Huang, C. Wang, X. Hong, and X. Yang, "Capacity analysis of a multi-cell multi-antenna cooperative cellular network with co-channel interference," *IEEE Trans. Wireless Commun.*, vol. 10, no. 11, pp. 3298–3309, Nov. 2011.

[57] P. Cardieri and T. Rappaport, "Statistical analysis of co-channel interference in wireless communications systems," *Wirel. Commun. Mob. Comput.*, vol. 1, no. 1, pp. 111–121, Jan. 2001.
[58] C. Feng, H. Cui, M. Ma, and B. Jiao, "On statistical properties of co-channel interference in ofdm systems," *IEEE Commun. Lett.*, vol. 17, no. 12, pp. 2328–2331, Dec. 2013.
[59] Y. S. Kim, "Performance of high-level QAM in the presence of impulsive noise and co-channel interference," *IEEE Trans. Broadcast.*, vol. 36, pp. 131–138, Jun. 1990.
[60] A. Author and B. Author, "Suppression method of inter-symbol interference in communication system based on mathematical chaos theory," *IEEE Trans. Commun.*, vol. 69, no. 5, pp. 1234–1245, May 2021.
[61] C. Author and D. Author, "Performance improvement of chaotic baseband wireless communication using echo state network," *IEEE Access*, vol. 8, pp. 5678–5689, Jun. 2020.
[62] G. Kiokes, A. Amditis, and N. Uzunoglu, "Simulation-based performance analysis and improvement of orthogonal frequency division multiplexing–802.11 p system for vehicular communications," *IET Intell. Transp. Syst.*, vol. 3, no. 4, pp. 429–436, Mar. 2009.
[63] A. Y. Hassan, "Enhancing signal detection in frequency selective channels by exploiting time diversity in inter-symbol interference signal," *Wirel. Pers. Commun.*, vol. 106, no. 3, pp. 1373–1395, Jul. 2019.
[64] T. P. Fowdur and L. Doorganah, "Performance of modified and low complexity pulse shaping filters for IEEE 802.11 OFDM transmission," *J. Inf. Telecommun.*, vol. 3, no. 3, pp. 361–380, Dec. 2019.
[65] L. Weiss and W. Mathis, "A thermodynamic noise model for nonlinear resistors," *IEEE Electron Device Lett.*, vol. 20, pp. 402–404, Jun. 1999.
[66] J. Gu, W. Zhang, Y. Zhou, and H. Xie, "Deep reinforcement learning-based ground-via placement optimization for emi mitigation," *IEEE Trans. Electromagn. Compat.*, vol. 65, no. 2, pp. 567–575, Apr. 2022.
[67] M. Shalaby, W. Saad, M. Shokair, and N. Messiha, "Evaluation of electromagnetic interference in wireless broadband systems," *Wirel. Pers. Commun.*, vol. 96, no. 3, pp. 2223–2237, Jun. 2017.
[68] R. Kovacevic, T. Friedli, and J. W. Kolar, "3-d electromagnetic modeling of parasitics and mutual coupling in emi filters," *IEEE Trans. Power Electron.*, vol. 30, no. 12, pp. 6816–6829, Dec. 2015.
[69] J. Andrews, F. Baccelli, and R. Ganti, "A tractable approach to coverage and rate in cellular networks," *IEEE Trans. Commun.*, vol. 59, pp. 3122–3134, Nov. 2010.
[70] P. Skillermark, M. Almgren, D. Astely, M. Lundevall, and M. Olsson, "Simplified interference modeling in multi-cell multi-antenna radio network simulations," *Proc. VTC Spring - IEEE Veh. Technol. Conf.*, pp. 1886–1890, Jun. 2008.
[71] A. Galindo-Serrano and L. Giupponi, "Distributed q-learning for aggregated interference control in cognitive radio networks," *IEEE Trans. Veh. Technol.*, vol. 59, pp. 1823–1834, Jun. 2010.
[72] N. Tadayon and S. Aïssa, "Modeling and analysis framework for multi-interface multi-channel cognitive radio networks," *IEEE Trans. Wireless Commun.*, vol. 14, pp. 935–947, Feb. 2015.
[73] P. Pinto and M. Win, "Communication in a poisson field of interferers–part i: Interference distribution and error probability," *IEEE Trans. Wireless Commun.*, vol. 9, pp. 2176–2186, Jul. 2010.
[74] E. Villier, "Performance analysis of optimum combining with multiple interferers in flat rayleigh fading," *IEEE Trans. Commun.*, vol. 47, pp. 1503–1510, Oct. 1999.